LANGMUIR

Article

pubs.acs.org/Langmuir

Differentiating Metastatic and Non-metastatic Tumor Cells from Their Translocation Profile through Solid-State Micropores

Waqas Ali,[†,‡,§] Azhar Ilyas,[†,‡,§,¶] Loan Bui,[∥] Bailey Sayles,[∥] Yeun Hur,[∥] Young-Tae Kim,[∥,⊥] and Samir M. Iqbal*[,†,‡,§,∥,⊥]

[†]Nano-Bio Lab, [‡]Department of Electrical Engineering, [§]Nanotechnology Research Center, and [∥]Department of Bioengineering, University of Texas at Arlington, Arlington, Texas 76019, United States

[⊥]Department of Urology, University of Texas Southwestern Medical Center at Dallas, Dallas, Texas 75235, United States

Supporting Information

ABSTRACT: Cancer treatment, care, and outcomes are much more effective if started at early stages of the disease. The presence of malignant cancer cells in human samples such as blood or biopsied tissue can be used to reduce overtreatment and underdiagnosis as well as for prognosis monitoring. Reliable quantification of metastatic tumor cells (MTCs) and non-metastatic tumor cells (NMTCs) from human samples can help in cancer staging as well. We report a simple, fast, and reliable approach to identify and quantify metastatic and non-metastatic cancer cells from whole biological samples in a point-of-care manner. The metastatic (MDA MB-231) and non-metastatic (MCF7) breast cancer cells were pushed through a solid-state micropore made in a 200 nm thin SiO_2 membrane while measuring current across the micropore. The cells generated very distinctive translocation profiles. The translocation differences stemmed from their peculiar mechanophysical properties. The detection efficiency of the device for each type of tumor cells was ~75%. MTCs showed faster translocation (36%) and 34% less pore blockage than NMTCs. The micropore approach is simple, exact, and quantitative for metastatic cell detection in a lab-on-a chip setting, without the need for any preprocessing of the sample.

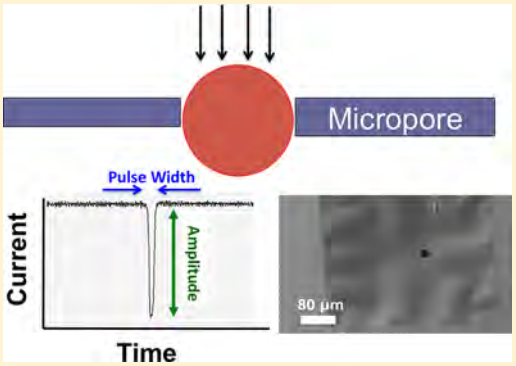

INTRODUCTION

Metastatic tumor cells (MTCs) and non-metastatic tumor cells (NMTCs) are both cancer derivatives of normal cells, but there are significant differences between the two.[1,2] These are different in their mechanophysical behavior, in their cytoskeleton structure, and the way they operate in a human body.[3−7] At the early stages of cancer, only NMTCs are dominant in a lesion but with time these cells start transforming into MTCs.[3,8] As the disease matures, the number of MTCs surpasses the number of NMTCs. Hence the advanced stages of cancer are marked by the abundant number of MTCs.[1,9] At any time, during the course of the disease, exact quantification of MTCs and NMTCs present in a human body can give a precise measure for the cancer stage and can indicate the maturity level of the disease.

It is important to determine the stage and monitor the progress for suitable therapy for all diseases. For cancer, this is of utmost importance. At early stages, many cancer types are dormant and curable. On the other hand, at the advanced stages, the disease is easily detectable but the chances of complete recovery are drastically reduced.[2,5] For instance, in the case of breast cancer, 5 year relative survival rate after breast cancer diagnosis and treatment is 93−100% for stage 0−2, but it significantly decreases to 22% for stage 4. Similarly, in the case of lung cancer, 5 year relative survival rate is 31% for stage 1, but it drops to 2% at stage 4. Therefore, it is very important to reliably and precisely detect any type of cancer in early stages (stage 1−2).[10] MTCs are much more dangerous and pose a greater health risk than NMTCs. These cells are the primary cause of 90% of the deaths of breast cancer patients.[11,12] Determining the exact ratio of MTCs and NMTCs present in cancer patients can be vital in prescribing the right cancer treatment. Though it is advantageous to quantify these two types of tumor cells from entire biological samples, at the same time, it is very challenging because there is no suitable technique to completely discriminate these cells in a point-of-care manner. All of the existing methods to investigate cell properties require labor-intensive preprocessing of the biological samples.[13] For example, magnetic twisting cytometry, atomic force microscopy, and micropipette aspiration have been shown to mechanically probe the cell surface, whereas microplate stretcher and laser/optical tweezers approaches do the same but optically.[13−18] All these assays require labor-intensive sample preparation, and none of these can claim assessment of every cell in the biological sample.[14,17,19] In a recent development engineered microbes have also been used to detect metastasis in liver.[20] It required oral delivery of the engineered probiotic to the patient followed by the analysis of

Received: January 4, 2016
Revised: March 24, 2016
Published: April 1, 2016

DOI: 10.1021/acs.langmuir.6b00016
Langmuir 2016, 32, 4924−4934

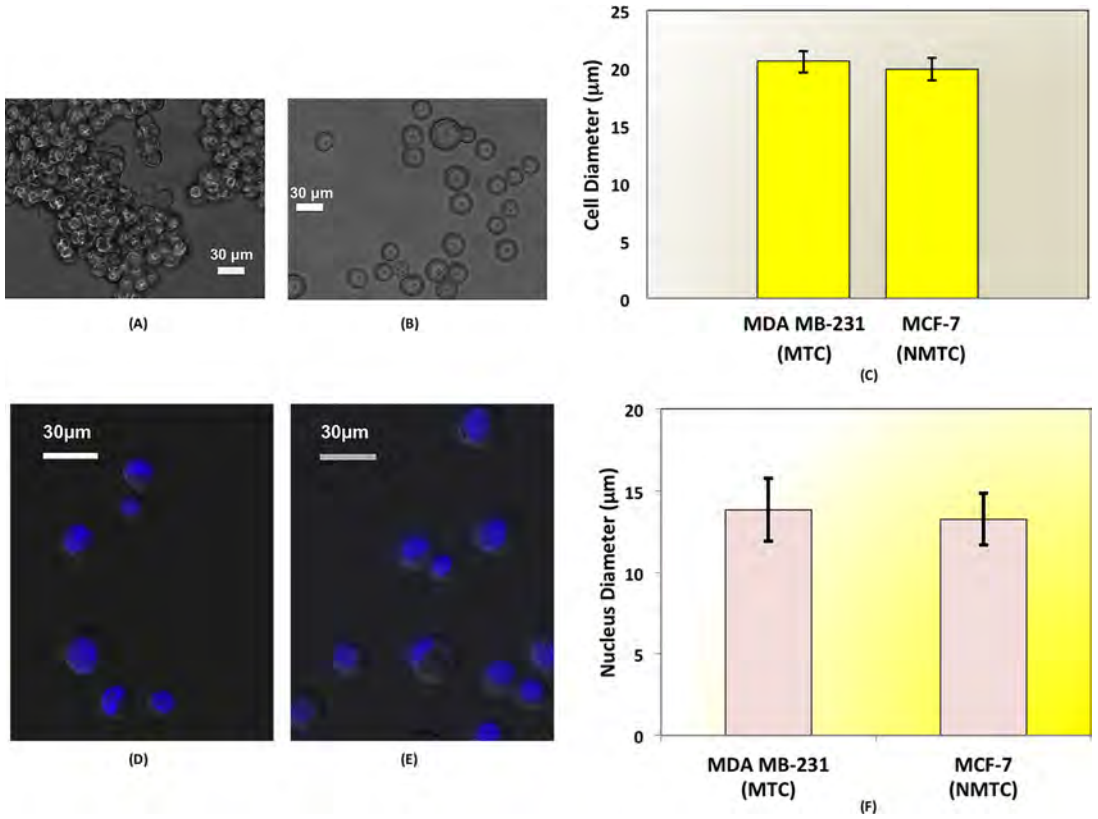

Figure 1. Cell and nucleus size comparison of the suspended (A) NMTCs (MCF7) and (B) MTCs (MDA MB-231). The cell diameter was measured from the optical images of cells (N = 30) of each tumor type, and average cell size was calculated. (C) The average cell size of MTCs and NMTCs was found to be very close. Average ± SD. Suspended MDA MB-231 and MCF-7 were stained for nuclei by incubating with Hoechst 33342 (Invitrogen) for 15 min at 37 °C. The fluorescence images of MTCs and NMTCs are shown in panels D and E, respectively. The nucleus diameter was measured based on the fluorescence images using *ImageJ*, and quantitative analysis (N = 30 per cell line) provided the average and standard deviation of the nucleus size shown in panel F.

the patient's urine sample. Bacterial diagnostic techniques such as this are still in their infancy, and there are several challenges such as selective trafficking of programmable probiotics, interaction of bacterial species, and so on that must be addressed before the clinical trial can be made possible. We report a simple and efficient electrical detection approach to distinguish MTCs and NMTCs directly from the blood/tissue sample based on their translocation profile through a solid-state micropore. A single micropore device is a resistive pulse sensor that works on the principle of a Coulter counter, in which any particle while translocating through the micropore causes a physical blockage which shows as a dip in the ionic current.[21] The travel of different species with different shapes and physical, mechanical, and chemical properties through the solid-state micropores causes unique electrical pulses in the ionic current.[22−25] Previously, a similar device was used to detect circulating tumor cells (CTCs) from the whole blood of a cancer patient.[26] That was primarily a size based detection scheme. Adamo et al. used a microfluidic device to relate the translocation time of cells through narrow constrictions with the cell stiffness and found that stiffer cells took longer to pass through when compared to less stiff ones, through the same diameter constriction.[27] They used Foster Shawn theory and an analogy with Coulter principle to infer that the cell diameter could be determined by measuring the cell travel time through the constriction up to a certain threshold. When the cell size was larger than the threshold value (i.e., when constriction was filled by the cell), the cell travel time became independent of the cell size. Only at this point did the device become sensitive to cell deformability.[27] Though there is not much difference between the cells' size as well as the size of the nuclei for MTCs and NMTCs, as shown in Figure 1, it has been reported that the two types of tumor cells differ significantly from each other in behavior and other cell properties.[2,5,28] NMTCs exhibit cell qualities similar to normal cells, whereas MTCs are more robust, dynamic, elastically deformable, and flexible.[2,16,28,29] Due to these differences, both types of cells give characteristic electrical signals while translocating through a micropore. NMTCs pass through the micropore slowly and cause much more ionic charge blockage whereas MTCs translocate much faster and exhibit less micropore blockage as indicated by their shorter dwell times and smaller peak amplitudes of the current pulses. This method provides a convenient and inexpensive way of differentiating MTCs and NMTCs in a lab-on-a-chip setting. It can be very useful for proper diagnosis of cancer and for prescribing the right treatment by detecting the maturity level of the disease. This method is free from preprocessing requirements and does not need any particle/bead attachment, surface functionalization, or fluorescent tagging.

■ EXPERIMENTAL SECTION

All chemicals were obtained from Sigma-Aldrich unless otherwise noted. All processes and methods were as per the approved institution policies.

Tumor Cell Interrogating Micropores. The micropores were fabricated with standard CMOS processing technology. A 4 in. double-

DOI: 10.1021/acs.langmuir.6b00016
Langmuir 2016, 32, 4924−4934

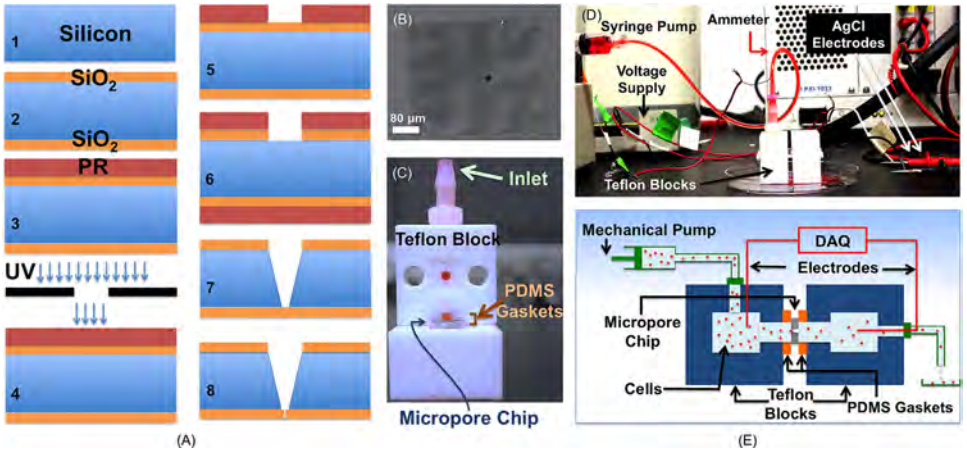

Figure 2. Device fabrication, assembly and cancer cell measurement setup. (A) Fabrication of silicon dioxide membranes using UV lithography followed by oxide and silicon etching in BHF and TMAH, respectively. The free-standing membrane of silicon dioxide is drilled with FIB to fabricate the micropores of 20 μm diameter. (B) SEM micrograph of a drilled micropore in the silicon dioxide membrane. (C) Micropore chip is sandwiched between two PDMS gaskets and held between two Teflon blocks. Each Teflon block has a reservoir; one is the inlet as shown and the other one is the outlet. (D) The micropore device is connected in series with the voltage supply and ammeter through Ag/AgCl electrodes. The Ag/AgCl electrodes are used to apply 5 V constant voltage and to measure the flow of ionic current through the micropore. (E) Micropore system schematic is shown.

side polished Si wafer of thickness 500 μm and orientation (100) was first oxidized to grow a thin silicon dioxide layer of 200 nm. The wafer was cleaned with Piranha solution (H_2SO_4:H_2O_2, 1:1) and spin-coated with positive photoresist (PR) (Shipley S1813) on one side. After spin-coating, the wafer was exposed to a UV source to pattern square etch windows on the spin-coated PR. The wafer was then dipped in developer solution (MF319) for a few seconds to remove the exposed PR. This step left patterned square windows in the PR through which the bare silicon dioxide was etched using buffered hydrofluoric acid (BHF) (Figure 2). During this process, the other side of the oxidized wafer was kept masked with a PR layer. The wafer was immersed in buffered hydrofluoric acid (BHF) to etch away the exposed silicon dioxide through the patterned PR window. At this point, the whole PR pattern was transferred to the underlying layer of oxide. After thorough rinsing with deionized (DI) water, the wafer was washed thoroughly with acetone to remove PR from both sides.

The wafer was immersed in 25% tetramethylammonium hydroxide (TMAH) at 90 °C to anisotropically etch silicon. TMAH etches silicon at a rate of ~1 μm/min.[30] After around 8 h, all of the silicon was etched away from the exposed area and etching ultimately stopped after reaching the oxide layer on the other side of the wafer. The whole wafer was then cut into 5 × 5 mm^2 chips using a dicing saw. Each chip had a membrane of silicon dioxide. Each chip was then drilled with a focused ion beam (FIB) to make micropores of 20 μm diameter. Diameters of drilled micropores can be controlled from 1 to 50 μm by adjusting exposure time, beam current, and acceleration voltage.[24,25] The micropores for this work were drilled using an acceleration voltage of 30 kV and beam current of 1 nA. The complete drilling occurred in 300 s for 200 nm thin oxide membranes. After drilling, each chip was annealed by exposing to very high temperatures for a few seconds to release mechanical stresses of the oxide membrane (Figure 2B).[25]

Measurement Setup and Data Analysis. The overall device assembly ensured that all paths for cell translocation were aligned and no solution leakage occurred. The micropore chip was sandwiched between two PDMS gaskets, and these gaskets were further sandwiched between two Teflon blocks (Figure 2C). PDMS gaskets properly sealed the micropore chip. The gaskets and both blocks had 1 mm holes, and the assembly was done in a way that the holes in the gaskets and blocks remained in alignment with the membrane in the chip. Both of the Teflon blocks had independent reservoirs that were connected to each other only through the micropore. One reservoir was the inlet and the other was the outlet, and both were filled with 0.85% (w/v) NaCl solution. Phosphate buffered saline (PBS) is a better medium for ensuring cell morphology, which was very crucial for these experiments. However, NaCl was used because the electrical signals were less noisy and conductivity change due to pore blockage was more prominent. The downside was that one must run the experiments within 1 h of suspending the cells in NaCl, otherwise the cell activity would degrade and the cells might die or loose their characteristics, causing them to become undistinguishable.

To apply voltage bias and to measure resulting current, Ag/AgCl electrodes were used. The electrodes were connected to the data acquisition cards (DAQ) and were dipped in each reservoir (Figure 2E). DAQ block included a digital multimeter (NI PXI-1033 and NI PXI-4071) and a DC voltage supply (NI SCB-68A, NI PXIe-6361, and NI SHC68-68-EPM). Cells were pushed into the inlet reservoir using a syringe pump (Harvard Apparatus). Micropore conductivity is given by the relation $G = \frac{\sigma\pi r^2}{L}$, where σ is the conductivity of NaCl solution, r is micropore radius, and L is the channel length/membrane thickness.[26] When cells passed through the micropore, these caused physical blockage of the micropore and reduced the effective radius that resulted in a decrease in conductivity. A LabView program was used to collect and store ionic current data which was further processed and analyzed with MATLAB scripts.[31] For statistical analysis, the average and the standard deviation were calculated and a t-test was carried out.

Flow Rate and Sampling Frequency. Special care had to be taken in selecting the flow rate of cells and the sampling frequency for micropore measurements. A very high flow rate would increase the device throughput but would be prone to miss subtle differences in translocation events between MTCs and NMTCs, hence causing the device to loose selectivity. A low flow rate would increase the device selectivity as there would be pronounced differences between the pulses from two types of cells, but the device throughput will deteriorate. Also using a very high sampling frequency adds too much noise to the system, decreasing the device sensitivity, but can potentially give higher resolution. A very small sampling frequency would have less noise, but it would result in missed translocation events, again reducing the sensitivity.[26] Taking these trade-offs into consideration, experiments were performed at a flow rate of 1 mL/h and sampling was done at 0.2 MHz.

Microchannel Device. The microchannels used in the cell migration experiment had height and length of 5 and 530 μm, respectively. The microchannel widths decreased from 20 μm to 15, 10, 8, and finally became 5 μm just before the receiving reservoir (Figures 3A,B). All devices were coated with collagen type 1 in

DOI: 10.1021/acs.langmuir.6b00016
Langmuir 2016, 32, 4924−4934

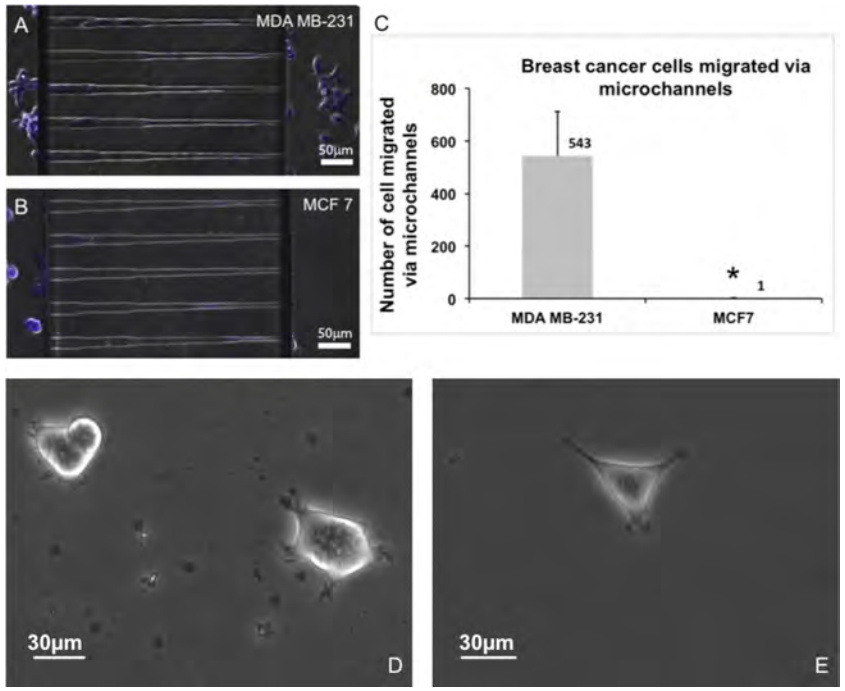

Figure 3. Quantitative comparison of migration ability between (A) MTCs and (B) NMTCs. Representative micrographs show migration through the tapered microchannels. (C) The panel shows the number of cells migrated from the seeding reservoir to the receiving reservoir via tapered microchannels; results are the average ± standard deviation (*$P < 0.01$). (D) MDA MB-231 cells growing on a cultured Petri dish were first imaged prior to passing through the micropore device. (E) After passing through the micropore, MDA MB-231 cells were collected, recultured on a Petri dish, and then imaged after 3 h. Comparison of the phenotype integrity was performed based on the morphology of the cells before and 3 h after passing through the micropore device.

advance. Dulbecco's modified Eagle's medium/F-12 medium with 10% fetal bovine serum (FBS) was used and renewed as necessary during cell culture.

The devices were incubated at 37 °C and in 5% CO_2 environment. The cells were allowed to migrate via microchannels for 96 h. After 96 h, the cells were fixed with 4% paraformaldehyde in 1X PBS and stained with DAPI. The cells that had migrated through the microchannels into the receiving reservoirs were then counted with a fluorescent microscope. For statistical analysis, the average and the standard deviation were calculated and a *t*-test was carried out.

Cell Culture. MDA MB-231 and MCF7 breast cancer cell lines and human fibroblast cell lines were obtained from the University of Texas Southwestern Medical Center (Dallas, TX). These cells were cultured in Dulbecco's modified Eagle's medium (DMEM/F-12, Cellgro, Corning) with 10% heat inactivated fetal bovine serum. Gentamycin and L-glutamine (Invitrogen) were also added to the cell culture medium. Human umbilical vein endothelial cells (HUVEC) were purchased from Lonza and cultured in Medium 200 (Life Technologies) supplemented with low serum growth supplement (LSGS, Life Technologies). The cells were cultured under sterile, humidified, 95% air, 5% CO_2, and 37 °C environment.

RESULTS

Cell Detection Efficiency. The experiments were repeated multiple times for both NMTCs and MTCs with known concentrations. Each peak in the data represented one cell. The number of peaks were used to calculate the detection efficiency of the device as follows.

$$\text{cell detection efficiency } (\eta) = \frac{\text{no. of cells detected}}{\text{total no. of cells}} \times 100\% \quad (1)$$

The efficiency was always more than ~75% for both cell types. Cell detection efficiency is strongly dependent on cell flow rate and sampling frequency, and changing any of these from their optimized values severely deteriorated the peak capture rate and hence the efficiency.

Electrical Signatures of MTCs and NMTCs. Separate solutions were prepared for each tumor cell type by suspending 10,000 cells of each in 10 mL of NaCl solution. Each mixture was processed for 40−60 min through a 20 μm micropore (Figure 2B) one after the other, and data were recorded at the optimized settings. Both types of cells caused significant current blockage while translocating through the micropore. The experiments were repeated thrice, and every time more than 75% cells were detected from the acquired pulses.

Analysis of the acquired data revealed that the distinguishing traits between the electrical pulses from the two tumor cells were the pulse width and pulse peak amplitude (Figure 4). Pulse width depicted the cell dwell time in the micropore. It was observed that the electrical pulses registered by NMTC translocations were significantly wider and deeper in contrast to those obtained from MTC translocations. NMTCs' registered pulses that had average peak amplitude of 5.85 μA (SD 0.57) and average pulse width of 155.74 μs (SD 10.19). On the contrary, the average peak amplitude and average width of the pulses obtained from MTCs translocation were 3.83 μA (SD 0.58) and 99.2 μs (SD 14.31), respectively (Figure 4). The 34% difference in peak amplitude and 36% difference in widths of the pulses were sufficient enough to uniquely identify these two tumor cell populations from their respective pulses.

Statistical data analysis was done by performing the *t*-test (unpaired). First, the test was conducted to check how significantly different were the registered pulses of NMTCs and MTCs in terms of their translocation times. The two populations ($N = 2000$) were found to be significantly different

DOI: 10.1021/acs.langmuir.6b00016
Langmuir 2016, 32, 4924−4934

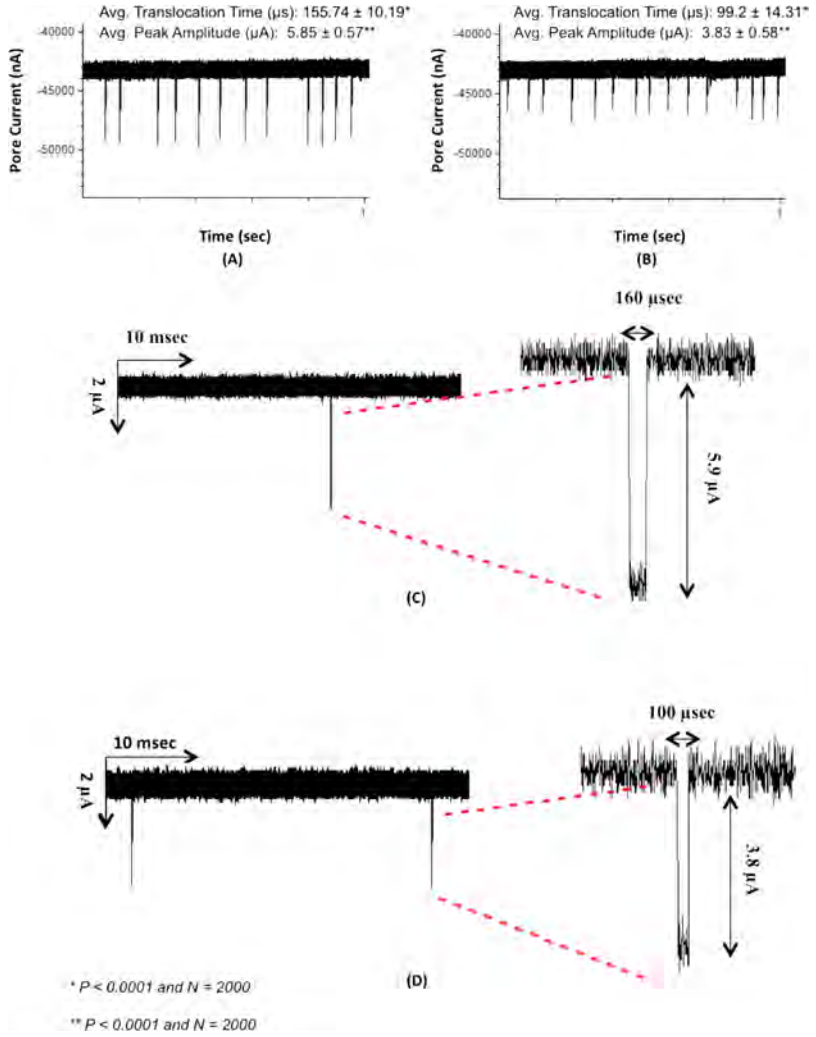

Figure 4. Temporal trace of ionic current showing pulses from the translocations of (A) NMTCs only and (B) MTCs only. Panels C and D show the ionic current profile of a representative pulse for NMTCs translocation and MTCs translocation, respectively. The characteristic pulse for NMTCs is wider and deeper, i.e., higher translocation time (~160 μs) and higher peak amplitude (~5.9 μA), whereas the characteristic pulse for MTCs is thinner (translocation time ~ 100 μs) and shallow (peak amplitude ~ 3.8 μA).

($p < 0.0001$). A similar test was conducted to check the discrimination efficiency of the registered pulses of NMTCs and MTCs in terms of their peak amplitude, and again the two populations ($N = 2000$) were found to be significantly different with $p < 0.0001$.

Reliability of Electrical Signatures from Micropore Device. The translocation profile was found to be steady throughout the measurements without any cell blockage. Figure 5 shows the comparison of electrical signal profiles for two cell types at three different time points (1, 10, and 30 min) of the recorded data. These results clearly demonstrated that the unique electrical signature of each cell reliably remained the same during the entire analysis period.

Quantitative Cellular Discrimination from a Mixture of NMTCs and MTCs. The count of MTCs is expected to be too few at the outset of metastasis. For a true application, this framework has to be able to distinguish relatively small concentrations of MTCs from NMTCs. It has been reported that on average as few as 5 CTCs are found in a 7.5 mL blood sample of breast cancer patients.[32] It is still a question of debate as to how many of these would go through mesenchymal–epithelial transition and extravasate and start a new tumor. In nude mice, as few as 100 tumor cells have been shown to start new tumors.[33] To this end, mixtures of NMTCs and MTCs with known concentrations of each cell type were processed with the micropore device. Both tumor cells were suspended in 10 mL of NaCl solution at two different relative concentrations (MTCs:NMTCs in 1:1 and 1:10). The solutions were mixed thoroughly to make homogeneous mixtures and were processed with the micropore device at a flow rate of 1 mL/h. The pulse counts for separate suspensions from the two mixtures are shown in Figure 6. The representative sample of 1 s for mixed suspension of equal concentrations of MTCs and NMTCs (1:1) shows four pulses for MTCs and seven pulses for NMTCs (Figure 6A) whereas the representative sample for mixed suspension of unequal concentrations of MTCs and NMTCs (1:10) shows one pulse for MTCs and 10 pulses for NMTCs in 1 s time duration (Figure 6B).

The detection efficiency for each cell type was again more than 75% and pulses were clearly distinguishable. Further analysis of the electrical pulses also indicated the presence of equal concentrations of both types of tumor cells for the 1:1 mixture. The second mixture contained 10,000 NMTCs and 1,000 MTCs (10:1). Again, the detection efficiency for each cell

DOI: 10.1021/acs.langmuir.6b00016
Langmuir 2016, 32, 4924–4934

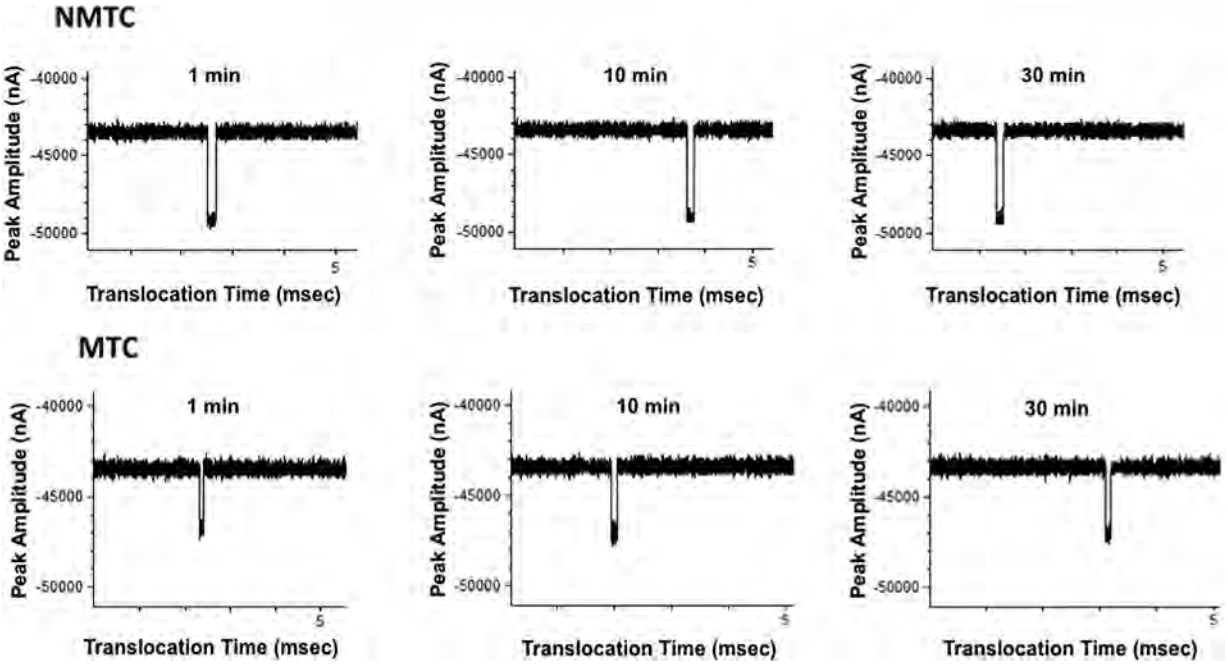

Figure 5. Stable translocation profile for both tumor cells throughout the experiments. The current signals at 1, 10, and 30 min after initial cell detection for each cell type are at the same baseline indicating the reliable operation of the device.

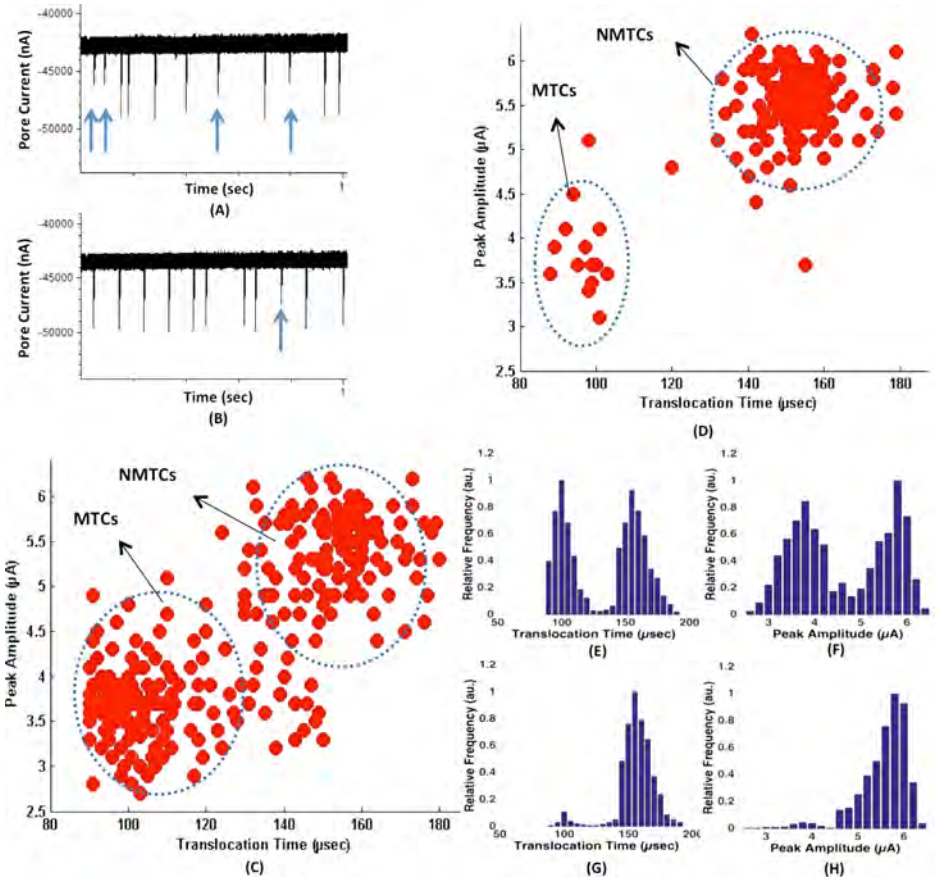

Figure 6. Temporal trace of the ionic current showing pulses from the translocations of MTCs and NMTCs in (A) 1:1 ratio (mixture 1) and (B) 1:10 ratio (mixture 2). Arrow indicates MTCs. Panels C and D show the data density scatter plot of pulse attributes from mixed cell suspensions of MTCs:NMTCs in 1:1 ratio and 1:10 ratio, respectively. In both C and D populations of MTCs and NMTCs obtained from pulse attributes are in line with the actual ratios of MTCs and NMTCs in the mixed suspensions. The distribution plots of translocation times and peak amplitudes for mixture 1 and mixture 2 are shown in panels E, F (1:1) and G, H (1:10), respectively. From the distribution plots, it can be seen that the variables (translocation time and peak amplitudes) are normally distributed.

DOI: 10.1021/acs.langmuir.6b00016
Langmuir 2016, 32, 4924−4934

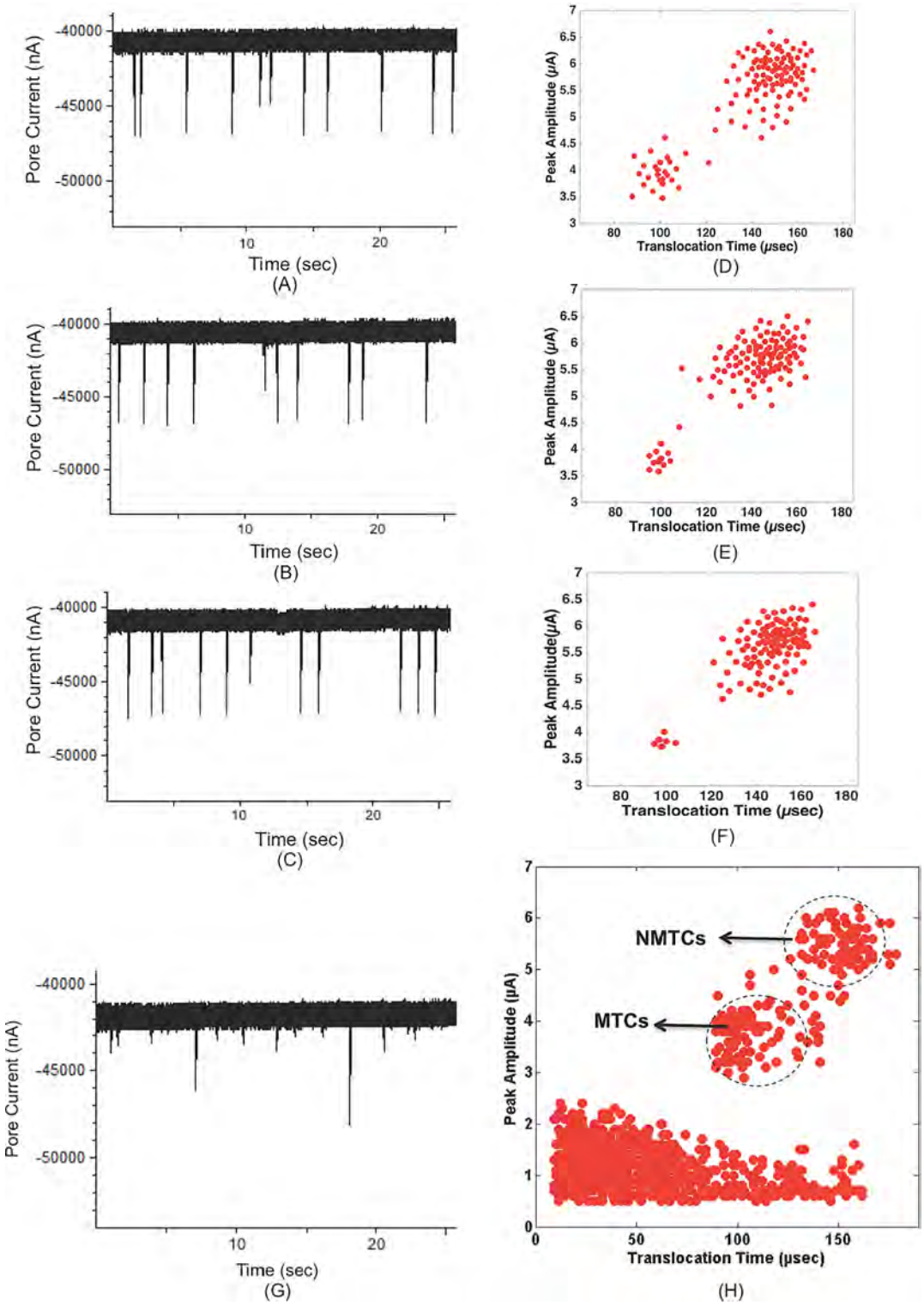

Figure 7. Temporal trace of the ionic current showing pulses from the translocation of three mixtures (10 mL each) containing a fixed number of NMTCs (10,000 cells) and MTCs [(A) 400 cells (1:25), (B) 200 cells (1:50), and (C) 100 cells (1:100)] and their corresponding scatter plots D, E, and F, respectively. Panels G and H show the temporal trace of the ionic current and scatter plot for the mixture of 5000 cells of endothelial cells and stromal fibroblasts each and 2000 cells of NMTCs and MTCs each.

type was more than 75% and the statistical analysis of the pulses revealed the presence of NMTCs and MTCs in ~10:1 ratio. The density plots, shown in Figure 6, indicate these results more clearly.

Statistical analysis was done by conducting the *t*-test. In Figure 6C, it can be seen that there are two populations. The one closer to the origin is of MTCs as these have shorter translocation times and peak amplitudes, and the one far from the origin is of NMTCs due to their longer translocation times and higher peak amplitudes. The *t*-test analysis revealed that the two populations were statistically different with respect to translocation times ($p < 0.0001$) as well as in peak amplitudes

DOI: 10.1021/acs.langmuir.6b00016
Langmuir 2016, 32, 4924−4934

Table 1. *t*-Test Analysis Results to Discriminate MTCs and NMTCs Population in a Limited Range

	t-test statistics to discriminate NMTCs and MTCs populations					
	with respect to the translocation time			with respect to the peak amplitude		
a	df	*t*-value	*p*-value	df	*t*-value	*p*-value
mixture 1: N_1 = 400; N_2 = 27	424	41.49	<0.0001	424	28.91	<0.0001
mixture 2: N_1 = 400; N_2 = 14	410	30.25	<0.0001	410	21.51	<0.0001
mixture 3: N_1 = 400; N_2 = 9	406	25.55	<0.0001	406	16.28	<0.0001

[a] N_1 = sample size for NMTCs; N_2 = sample size for MTCs.

($p < 0.0001$). Further, it can be seen from the plot that the two distinct populations have almost the same population density, which indicates the presence of an equal number of NMTCs and MTCs in the mixture. Also, in Figure 6D, there are two distinct populations. The population close to the origin has much lower density as compared to the other one indicating the presence of fewer MTCs than NMTCs (1:10). The *t*-test analysis revealed that the two populations were significantly different with respect to translocation times ($p < 0.0001$) as well as peak amplitudes ($p < 0.0001$). These results indicate that precise quantification of NMTCs and MTCs can be done in a mixture. All of the experiments were done in triplicate. The data shown here are representative of the trends of other runs.

Detection Limit. To determine the limit of detection of the micropore device, a series of translocation experiments were conducted. For these experiments, three mixtures of MTCs and NMTCs were prepared in 10 mL of NaCl solution each. The cell count of NMTCs was kept fixed at 10,000 cells for all three mixtures whereas the cell count for MTCs was gradually reduced. The first mixture had 400 MTCs, the second had 200, and the third mixture contained only 100 MTCs. The temporal traces of the ionic current and the scatter plots for mixtures 1, 2, and 3 are shown in Figure 7A–F, respectively. In 1 h, 1 mL of solution translocated through the micropore for each mixture and MTCs were detected reliably for each mixture. To check the discrimination efficiency of the two populations, i.e., one from NMTCs and one from MTCs, in terms of their respective translocation times and peak amplitudes, the *t* test was conducted. The test results for the three mixtures are shown in Table 1. From the test results it was inferred that the micropore device could easily detect MTCs even if these were as low as 10 cells/mL. It is also possible to detect even a lower concentration of MTCs than 10 cells/mL through this micropore device, but then we would need to make sure that no cells cluster together in the suspension. This would require the addition of a chemical agent in the mixture that would break the EpCAM and hence reduce the chances of cell agglomeration. This limit of detection is very much in line with the real sample wherein MTCs as few as 100 are known to develop tumors in immunocompromised host mice.[33]

Cellular Discrimination from an Impure Sample. In the actual patient samples, there are many other cells than just MTCs and NMTCs. White blood cells (WBCs), red blood cells (RBCs), endothelial cells, and fibroblasts are a few of these. Since it has already been established that tumor cells can be differentiated from the WBCs and RBCs through the micropore device,[26] it was more important to make sure that cells such as endothelial and fibroblasts did not interfere with the detection of MTCs and NMTCs through the micropore device. To demonstrate the feasibility of this device for processing of actual patient samples, a mixture of human umbilical vein endothelial cells (HUVEC), human fibroblasts, MTCs, and NMTCs was prepared by mixing 5000 cells of endothelial cells and fibroblasts each and 2000 cells of MTCs and NMTCs each, in 10 mL of NaCl solution. The mixture was processed through the micropore for 1 h. A representative sample of the registered pulses is shown in Figure 7G, and the scatter plot of the registered events is shown in Figure 7H. Quantitatively, there are no direct ways to compare the number of rare subpopulations within tumors that may form secondary tumors but a thousand of breast tumorigenic cells have been known to form tumors when injected into the mammary fat pad of SCID mice.[33]

The sizes of endothelial cells and fibroblasts are around 13 μm and 10–15 μm, respectively.[34−37] The translocation of these cells through a 20 μm micropore caused pulses that were very different from those of MTCs and NMTCs. The translocation time of the pulses registered due to the translocation of endothelial cells and fibroblasts ranged from around 15 μs up to 150 μs, but the majority of the population was centered around 40 μs. The peak amplitude of the pulses was in the range of 0.7–2 μA. It can be clearly seen from Figure 7H that MTCs and NMTCs can still be detected from the sample and can be differentiated from each other without any problem since the pulses associated with MTCs and NMTCs are significantly different than those of endothelial cells and stromal fibroblasts.

Breast Cancer Cell Migration through Tightly Confined Microchannels. To further investigate the mechanical differences between two cell types, and to see whether the translocation difference was indeed due to the difference in mechanical nature of the two cell types, cell migration was also observed through tightly confined microchannels. The MTCs and NMTCs were separately seeded (10,000 cells/device; n = 18 devices/each cell type) in a microchannel device as described elsewhere.[38] The device design had two reservoirs, one to seed the cells and another to receive them through tapered microchannels.

MTCs had an average of 542.3 ± 168.8 cells that completely migrated to the receiving reservoir in contrast to an average of 1.22 ± 1.66 NMTCs as shown in Figure 3C. This clearly showed that MTCs had the ability to quickly move through tightly confined microchannels such as micropores whereas NMTCs were challenged by the spatial confinement.

DISCUSSION

Elastic deformability differences between non-metastatic breast cancer cells and metastatic breast cancer cells were exploited to electrically differentiate NMTCs and MTCs with the use of micropores. Since the syringe pump pushed the sample from the inlet toward the outlet at a stable rate of 1 mL/h, both MTCs and NMTCs were forced to pass through the micropore, the size of which was deliberately kept smaller than both types of tumor cells. The reason is that, to investigate

DOI: 10.1021/acs.langmuir.6b00016
Langmuir 2016, 32, 4924−4934

the elastic deformability as a discriminating factor between two types of tumor cells, they should deform to pass through the micropore that is only possible when the micropore size is smaller than the tumor cell size. Table 2 shows the calculated values of shear rate, shear stress, and velocity of cells inside and in the vicinity of the micropore, and for comparison these values for blood inside the arteries and veins of a human body have also been noted here.[39] For calculations, the liquid medium (NaCl) was assumed to be a Newtonian fluid. Inside the micropore, the values are orders of magnitude higher than that of arteries and veins as well as the micropore vicinity that is primarily because of the size difference between arteries ($d \sim 4$ mm), veins ($d \sim 5$ mm), and micropore ($d \sim 20$ μm). Shear stress and shear rate are strong functions of the size of the flow path. A very high value of shear rate inside the micropore implies that a very high degree of deformability is induced in cells while translocating through the micropore which is an indication that the translocation profile is a true reflection of the deformability properties of the cells.

Table 2. Comparison of Shear Rate, Shear Stress and Velocity of Fluid Inside and Just Outside the Micropore with Those for Blood in Arteries and Veins[39]

	arteries	veins	micropore	micropore vicinity
shear rate (s^{-1})	900	160	3.53×10^8	353
shear stress (dyn/cm^2)	4−30	1−4	3.53×10^6	3.53
velocity (m/s)	0.45	0.1	882	0.088

Cell deformability is directly linked to the elasticity of the cells. Staunton et al. have reported a 4-fold elasticity difference between the cellular deformability of metastatic cells and their non-metastatic counterparts.[1] Byun et al. also demonstrated the nexus between deformability of cells and their metastatic potential.[40] They reported the reduced friction of cancer cells as another factor for their enhanced metastatic potential and demonstrated that cell entrance velocity into a narrow constriction was an indicator of their deformability whereas cell transit velocity indicated whether the cell offered reduced friction or not while traveling through a narrow constriction. Metastatic cells are known to be more elastically deformable and softer, and these are capable of exerting increased force.[28,39,41,42] While translocating through the micropore, both NMTCs and MTCs deformed to adjust to the size of the micropore. A lower translocation time for MTCs as compared to NMTCs stands to reason. Since MTCs are known to depict higher elastic deformability and are more pliable than the NMTCs, they took less time to deform and adjust according to the micropore size. On the other hand, NMTCs took comparatively longer time to deform due to their lower elasticity and hence hindered the ionic flow through the micropore for a longer time yielding a higher translocation time. The more time a cell takes to deform and adjust to the size of micropore, the longer it will hinder the ionic flow through the micropore and ultimately will result in a higher translocation time and vice versa. So the cell translocation time is an indirect measure of the cell elasticity. Due to higher cell elasticity, MTCs spent less time in the micropore because these could squeeze through more easily than NMTCs, which were rigid. The two cell types are known to have different elastic moduli (341 ± 41 Pa for MTC and 425 ± 31 Pa for NMTC)[43] as well as drastically different levels of strain energy when measured in an elastic matrix (∼0.8 pJ for MTCs vs ∼0.4 pJ for NMTC).[44] The two tumor cell types are also known to have different properties of motility. Metastatic cells are capable of traveling farther and in a spontaneous manner whereas non-metastatic cells are inclined to move in a nonlinear manner.[4,28,29] With the fact that the nuclei are much more stiff and viscous than the surrounding cytoplasm, the nuclei are also possibly contributing to the resulting differences in the behavior.[45] These known cell traits of MTCs and NMTCs are also in line with our experimental observations and support our findings.

It is also important that experimental conditions do not affect the phenotype of the cells so that postprocessing and standard cytometry can be done later on. In this regard, one might think that very high values of shear rate and velocity of fluid inside the micropore may jeopardize the phenotype of translocating cells, rendering them useless for postprocessing. Luckily this is not the case, and such a high velocity and shear rate in the micropore did not affect the cell microenvironment and the cells stayed in their native state. Comparison of the phenotype integrity was performed based on the morphology of the cells before and 3 h after passing through the micropore device (Figure 3D,E). MDA MB-231 cells growing on a cultured Petri dish were first imaged prior to passing through the micropore device. Then after passing through the micropore, MDA MB-231 cells were collected, recultured on a Petri dish, and then imaged again after 3 h. As can be seen in Figure 3E, the cells did not show any change in their morphology. The rapid transaction through the micropore made the cell boundary squeeze only for so small a time that the internal rearrangement was for a very short transient. For the rest of the time, when cells were not inside the micropore, these experienced shear rate and velocity very close to what these would experience in arteries and veins of the human body (Table 2). These cells thus did not undergo any change in their phenotype and can be used for postprocessing and standard cytometry. Postprocessing can tell us a lot about new genes and cellular pathways that have been involved in the metastasis.

Micropore devices have been used as a filter in the past for size based detection of cells and their 3D profiling,[27,46] but in this work we have demonstrated its use as an electromechanical transducer. More recently micropore device has been used to differentiate different types of lung cancer cells using the same principle.[47] Our micropore device works as a transducer that probes the mechanophysical properties of the translocating cells and generates electrical pulses based on those properties. These pulses can be analyzed then for cell differentiation and quantification. This whole process, i.e., from the time when patient samples are collected until the analysis is completed using this device, takes not more than 1−2 h and that too without the aid of specialized equipment and well-trained staff or physicians. All that is needed to get the timely results is a micropore device and the accompanying data acquisition and analysis setup that can be used for patient's diagnoses in an ambulance, in the physician's office or home, or in a hospital. The presented scheme is not limited to breast cancer but is also suitable for differentiating any types of cells which differ in their biomechanical properties such as stiffness, viscosity, elastic deformability, and shape, etc. This approach has the potential to empower physicians to make timely decisions at the "point-of-care" and will help fight cancer in a better way. It can also be very useful in cancer therapy monitoring as cancer therapists almost always need to stage the cancer to determine outcomes

DOI: 10.1021/acs.langmuir.6b00016
Langmuir 2016, 32, 4924−4934

and prognosis. Presence of more MTCs would indicate an advanced cancer stage. This device can conveniently be used to get these results quickly and reliably in a lab-on-a chip setting.

■ ASSOCIATED CONTENT

Supporting Information

The Supporting Information is available free of charge on the ACS Publications website at DOI: 10.1021/acs.langmuir.6b00016.

Images showing additional experimental runs of translocation of mixtures of NMTCs and MTCs correlated to those of Figure 4, Figure 6, and Figure 7 (PDF)

■ AUTHOR INFORMATION

Corresponding Author

*E-mail: SMIQBAL@uta.edu. Tel.: 817-272-0228. Fax: 817-272-7458.

Present Address

¶Azhar Ilyas, Department of Biomedical Sciences, Texas A&M University, Baylor College of Dentistry, Dallas, TX 75246, USA.

Notes

The authors declare no competing financial interest.

■ ACKNOWLEDGMENTS

We thank M. U. Raza, M. Arif I. Mahmood, M. M. Bellah, and M. Islam for their help and useful discussions during this work. We also thank the staff at Nanotechnology Research Center at UTA for training at various stages and thank Dr. Robert Bachoo at UT Southwestern Medical center for providing us the breast cancer cells. The work was supported by NSF Grant ECCS-1201878 and CPRIT Grant RP110041.

■ REFERENCES

(1) Agus, D. B.; et al. A Physical Sciences Network Characterization of Non-tumorigenic and Metastatic Cells. *Sci. Rep.* **2013**, *3*, 1449.

(2) Chaffer, C. L.; Weinberg, R. A. A Perspective on Cancer Cell Metastasis. *Science* **2011**, *331*, 1559−1564.

(3) Chambers, A. F.; Groom, A. C.; MacDonald, I. C. Dissemination and growth of cancer cells in metastatic sites. *Nat. Rev. Cancer* **2002**, *2*, 563−572.

(4) Ward, K. A.; Li, W. I.; Zimmer, S.; Davis, T. Viscoelastic properties of transformed cells: Role in tumor cell progression and metastasis formation. *Biorheology* **1991**, *28*, 301−313.

(5) Sahai, E. Illuminating the metastatic process. *Nat. Rev. Cancer* **2007**, *7*, 737−749.

(6) Suresh, S. Biomechanics and biophysics of cancer cells. *Acta Mater.* **2007**, *55*, 3989−4014.

(7) Chakraborty, J.; Von Stein, G. A. Pleomorphism of human prostatic cancer cells (DU 145) in culture–the role of cytoskeleton. *Exp. Mol. Pathol.* **1986**, *44*, 235−245.

(8) Gao, Y.; Xie, J.; Chen, H.; Gu, S.; Zhao, R.; Shao, J.; Jia, L. Nanotechnology-based intelligent drug design for cancer metastasis treatment. *Biotechnol. Adv.* **2014**, *32*, 761−777.

(9) Yoshioka, S.; et al. [The efficacy of early diagnosis of brain metastasis and systemic treatment after radiotherapy in patients with metastatic breast cancer]. *Gan To Kagaku Ryoho* **2013**, *40*, 2381−2383.

(10) Jemal, A.; Siegel, R.; Ward, E.; Hao, Y.; Xu, J.; Murray, T.; Thun, M. J. Cancer statistics, 2008. *Ca-Cancer J. Clin.* **2008**, *58*, 71−96.

(11) Scully, O. J.; Bay, B.-H.; Yip, G.; Yu, Y. Breast Cancer Metastasis. *Cancer Genomics Proteomics* **2012**, *9*, 311−320.

(12) Marino, N.; Woditschka, S.; Reed, L. T.; Nakayama, J.; Mayer, M.; Wetzel, M.; Steeg, P. S. Breast cancer metastasis: issues for the personalization of its prevention and treatment. *Am. J. Pathol.* **2013**, *183*, 1084−1095.

(13) Kuttel, C.; Nascimento, E.; Demierre, N.; Silva, T.; Braschler, T.; Renaud, P.; Oliva, A. G. Label-free detection of babesia bovis infected red blood cells using impedance spectroscopy on a microfabricated flow cytometer. *Acta Trop.* **2007**, *102*, 63−68.

(14) Binnig, G.; Quate, C. F.; Gerber, C. Atomic force microscope. *Phys. Rev. Lett.* **1986**, *56*, 930−933.

(15) Hessler, J. A.; Budor, A.; Putchakayala, K.; Mecke, A.; Rieger, D.; Banaszak Holl, M. M.; Orr, B. G.; Bielinska, A.; Beals, J.; Baker, J., Jr. Atomic force microscopy study of early morphological changes during apoptosis. *Langmuir* **2005**, *21*, 9280−9286.

(16) Sleep, J.; Wilson, D.; Simmons, R.; Gratzer, W. Elasticity of the red cell membrane and its relation to hemolytic disorders: an optical tweezers study. *Biophys. J.* **1999**, *77*, 3085−3095.

(17) Evans, E. A. New membrane concept applied to the analysis of fluid shear- and micropipette-deformed red blood cells. *Biophys. J.* **1973**, *13*, 941−954.

(18) Mills, J. P.; Qie, L.; Dao, M.; Lim, C. T.; Suresh, S. Nonlinear elastic and viscoelastic deformation of the human red blood cell with optical tweezers. *MCB: Mech. Chem. Biosyst.* **2004**, *1*, 169−180.

(19) Dao, M.; Lim, C. T.; Suresh, S. Mechanics of the human red blood cell deformed by optical tweezers. *J. Mech. Phys. Solids* **2003**, *51*, 2259−2280.

(20) Danino, T.; Prindle, A.; Kwong, G. A.; Skalak, M.; Li, H.; Allen, K.; Hasty, J.; Bhatia, S. N. Programmable probiotics for detection of cancer in urine. *Sci. Transl. Med.* **2015**, *7* (289), 289ra84.

(21) Saleh, O. A.; Sohn, L. L. Quantitative sensing of nanoscale colloids using a microchip coulter counter. *Rev. Sci. Instrum.* **2001**, *72*, 4449.

(22) Ilyas, A.; Asghar, W.; Ahmed, S.; Lotan, Y.; Hsieh, J.-T.; Kim, Y.-t.; Iqbal, S. M. Electrophysiological analysis of biopsy samples using elasticity as an inherent cell marker for cancer detection. *Anal. Methods* **2014**, *6*, 7166−7174.

(23) Venkatesan, B. M.; Bashir, R. Nanopore sensors for nucleic acid analysis. *Nat. Nanotechnol.* **2011**, *6*, 615−624.

(24) Asghar, W.; Ilyas, A.; Deshmukh, R. R.; Sumitsawan, S.; Timmons, R. B.; Iqbal, S. M. Pulsed plasma polymerization for controlling shrinkage and surface composition of nanopores. *Nanotechnology* **2011**, *22*, 285304.

(25) Asghar, W.; Ilyas, A.; Billo, J. A.; Iqbal, S. M. Shrinking of solid-state nanopores by direct thermal heating. *Nanoscale Res. Lett.* **2011**, *6*, 372.

(26) Asghar, W.; Wan, Y.; Ilyas, A.; Bachoo, R.; Kim, Y. T.; Iqbal, S. M. Electrical fingerprinting, 3D profiling and detection of tumor cells with solid-state micropores. *Lab Chip* **2012**, *12*, 2345−2352.

(27) Adamo, A.; Sharei, A.; Adamo, L.; Lee, B.; Mao, S.; Jensen, K. F. Microfluidics-based assessment of cell deformability. *Anal. Chem.* **2012**, *84*, 6438−6443.

(28) Swaminathan, V.; Mythreye, K.; O'Brien, E. T.; Berchuck, A.; Blobe, G. C.; Superfine, R. Mechanical stiffness grades metastatic potential in patient tumor cells and in cancer cell lines. *Cancer Res.* **2011**, *71*, 5075−5080.

(29) Fraley, S. I.; Feng, Y.; Krishnamurthy, R.; Kim, D. H.; Celedon, A.; Longmore, G. D.; Wirtz, D. A distinctive role for focal adhesion proteins in three-dimensional cell motility. *Nat. Cell Biol.* **2010**, *12*, 598−604.

(30) Tabata, O.; Asahi, R.; Funabashi, H.; Shimaoka, K.; Sugiyama, S. Anisotropic etching of silicon in TMAH solutions. *Sens. Actuators, A* **1992**, *34*, 51−57.

(31) Billo, J. A.; Asghar, W.; Iqbal, S. M. An implementation for The detction and analysis of negative peaks in an applied current signal across a silicon nanopore. *Proc. SPIE* **2011**, *8031*, 80312T−80312T-80317.

(32) Cristofanilli, M.; et al. Circulating tumor cells, disease progression, and survival in metastatic breast cancer. *N. Engl. J. Med.* **2004**, *351*, 781−791.

(33) Ponti, D.; Costa, A.; Zaffaroni, N.; Pratesi, G.; Petrangolini, G.; Coradini, D.; Pilotti, S.; Pierotti, M. A.; Daidone, M. G. Isolation and

DOI: 10.1021/acs.langmuir.6b00016
Langmuir 2016, 32, 4924−4934

in vitro propagation of tumorigenic breast cancer cells with stem/progenitor cell properties. *Cancer Res.* **2005**, *65*, 5506−5511.
(34) Garipcan, B.; Maenz, S.; Pham, T.; Settmacher, U.; Jandt, K. D.; Zanow, J.; Bossert, J. Image analysis of endothelial microstructure and endothelial cell dimensions of human arteries - a preliminary study. *Adv. Eng. Mater.* **2011**, *13*, B54−B57.
(35) Iwanaga, K.; Murata, T.; Hori, M.; Ozaki, H. Isolation and characterization of bovine intestinal subepithelial myofibroblasts. *J. Pharmacol. Sci.* **2010**, *112*, 98−104.
(36) Brouty-Boye, D.; Mainguene, C.; Magnien, V.; Israel, L.; Beaupain, R. Fibroblast-mediated differentiation in human breast carcinoma cells (MCF-7) grown as nodules in vitro. *Int. J. Cancer* **1994**, *56*, 731−735.
(37) Kusuhara, M.; Yamaguchi, K.; Nagasaki, K.; Hayashi, C.; Suzaki, A.; Hori, S.; Handa, S.; Nakamura, Y.; Abe, K. Production of endothelin in human cancer cell lines. *Cancer Res.* **1990**, *50*, 3257−3261.
(38) Wan, Y.; Tamuly, D.; Allen, P. B.; Kim, Y. T.; Bachoo, R.; Ellington, A. D.; Iqbal, S. M. Proliferation and migration of tumor cells in tapered channels. *Biomed. Microdevices* **2013**, *15*, 635−643.
(39) Wirtz, D.; Konstantopoulos, K.; Searson, P. C. The physics of cancer: the role of physical interactions and mechanical forces in metastasis. *Nat. Rev. Cancer* **2011**, *11*, 512−522.
(40) Byun, S.; et al. Characterizing deformability and surface friction of cancer cells. *Proc. Natl. Acad. Sci. U. S. A.* **2013**, *110*, 7580−7585.
(41) Fuchs, E.; Weber, K. Intermediate filaments: structure, dynamics, function, and disease. *Annu. Rev. Biochem.* **1994**, *63*, 345−382.
(42) Zhu, C.; Bao, G.; Wang, N. Cell mechanics: mechanical response, cell adhesion, and molecular deformation. *Annu. Rev. Biomed. Eng.* **2000**, *2*, 189−226.
(43) Jonas, O.; Mierke, C. T.; Kaes, J. A. Invasive cancer cell lines exhibit biomechanical properties that are distinct from their non-invasive counterparts. *Soft Matter* **2011**, *7*, 11488−11495.
(44) Koch, T. M.; Muenster, S.; Bonakdar, N.; Butler, J. P.; Fabry, B. 3D traction forces in cancer cell invasion. *PLoS One* **2012**, *7*, e33476.
(45) Lim, C. T.; Zhou, E. H.; Quek, S. T. Mechanical models for living cells–a review. *J. of Biomech.* **2006**, *39*, 195−216.
(46) Ilyas, A.; Asghar, W.; Kim, Y. T.; Iqbal, S. M. Parallel recognition of cancer cells using addressable array of solid-state micropores. *Biosens. Bioelectron.* **2014**, *62*, 343−349.
(47) Ali, W.; Moghaddam, F. J.; Raza, M. U.; Bui, L.; Sayles, B.; Kim, Y. T.; Iqbal, S. M. Electromechanical transducer for rapid detection, discrimination and quantification of lung cancer cells. *Nanotechnology* **2016**, *27*, 195101.

DOI: 10.1021/acs.langmuir.6b00016
Langmuir 2016, 32, 4924−4934